Unoccupied electronic states and surface barriers at Cu surfaces

1993 J. Phys.: Condens. Matter 5 599

(http://iopscience.iop.org/0953-8984/5/5/011)

J. Phys.: Condens. Matter 5 (1993) 599–614. Printed in the UK

Unoccupied electronic states and surface barriers at Cu surfaces

M Graß†, J Braun†, G Borstel†, R Schneider‡, H Dürr‡, Th Fauster‡ and V Dose‡

† Fachbereich Physik, Universität Osnabrück, D-4500 Osnabrück, Germany
‡ Max-Planck-Institut für Plasmaphysik, D-8046 Garching, Germany

Received 22 October 1992

Abstract. The surface potential barrier shape of the low-index faces of copper was determined by an analysis of inverse photoemission and two-photon photoemission measurements making use of the one-step model of photoemission. The barrier potentials obtained in this way allow for a consistent description of the energetic positions and effective masses of all known surface states for the various faces. It is found, in agreement with previous theoretical predictions, that the most open surface, Cu(110), exhibits the strongest saturation of the image potential with an image plane lying nearest to the topmost atomic layer and with the weakest image force outside the crystal. A comparison with theoretical slab calculations shows that in these calculations the position of the image plane is always significantly further outside the crystal than derived in the present study. Dynamical effects in the effective potential are found to be negligible for electronic states up to 6 eV above the Fermi level E_F, but are probably responsible for systematic discrepancies between theory and experiment for unoccupied bulk states in the energy range 10–15 eV above E_F.

1. Introduction

Inverse photoemission (IPE), two-photon photoemission (2PPE) and very-low-energy electron diffraction (VLEED) have recently led to a renewed interest in the study of unoccupied electronic surface states in the local energy gaps of metals. In this context the variation of the potential near the metal–vacuum interface has been central to the discussions.

The effective potential felt by an electron in the surface region is mediated by the electrons self-energy $\Sigma(r, r', E)$, which represents a non-Hermitean, non-local, energy-dependent operator [1]. The self-energy Σ is usually defined within the Green function formalism of elementary excitations in interacting many-particles systems in such a way, that it takes into account all the dynamical exchange and correlation effects beyond the Hartree approximation [2]. For electron states exactly at the Fermi level E_F, it can be shown in the framework of density functional theory (DFT), that the total effect of $\Sigma(r, r', E_F)$ can be incorporated exactly by means of an effective local static potential $V_{XC}(r)$ [3]. Within the usual local density approximation (LDA) for $V_{XC}(r)$ DFT allows for an *ab-initio* calculation of the total effective potential, which near the metal-vacuum interface is then termed the surface barrier potential $V_B(r)$ [4].

0953-8984/93/050599+16$07.50

For occupied and unoccupied electronic surface states at metals with energies near E_F the DFT surface barrier V_B in principle gives an excellent description. Unfortunately, however, the LDA in DFT results in an incorrect asymptotic behaviour of $V_B(r)$ in the vacuum region. For large distances $|z|$ from the metal surface $V_B(r)$ in LDA decays exponentially, instead of behaving proportional to $|z|^{-1}$, which in turn is required by simple electrostatic arguments. This shortcoming of the usual LDA–DFT barrier potential has led some authors to work in practical calculations with parametrized models for the surface barrier.

In this contribution we study occupied and unoccupied surface states at the three low-index surfaces of Cu. We will use a parametrized surface barrier and calculate both the energetics and corresponding IPE spectra for surface states on the basis of the dynamical one-step model of photoemission [5–7].

The aim of this paper is to extract as much information as possible about the barrier potential of Cu by comparing our calculated results with the wealth of experimental information on Cu surface states available in the literature.

2. One-step model: surface contribution

The general theory for the surface contribution in the one-step model has already been described in a very compact form elsewhere [8]. In the following we present the full details of its derivation. For a clean and unreconstructed surface the effective static barrier potential takes the form [9],

$$V_B(r) = \sum_g V_{Bg}(z) e^{ig \cdot r_\parallel}. \tag{1}$$

Here g denotes a two-dimensional reciprocal lattice vector and $r_\parallel$ is parallel to the surface. Self-consistent electronic structure calculations for solid metal films in the framework of DFT [4] have demonstrated that $V_B(r)$ has a distinctly three-dimensional character. The periodic variation of V_B in the lateral directions is commonly referred to as corrugation. At the present level of accuracy in VLEED and IPE corrugation effects seem, however, to be of relative insignificance [10, 11]. Thus all terms with $g \neq 0$ in (1) are usually disregarded and V_B is approximated in one-dimensional form $V_B(z)$.

In the framework of the one-step model of angular resolved ultraviolet photoemission (ARUPS) and inverse photoemission [5–7] the electron (photon) current is described by the following expression:

$$I(k_\parallel, \epsilon_f) = -(1/\pi)\mathrm{Im}\langle k_\parallel, \epsilon_f | G_2^+ \Delta G_1^+ \Delta^\dagger G_2^- | \epsilon_f, k_\parallel \rangle. \tag{2}$$

The propagators for the final- and for the hole-state are denoted by $G_2^\pm$ and G_1^+, respectively, and calculated from standard layer Korringa–Kohn–Rostoker (KKR) multiple scattering techniques for the semi-infinite crystal [5, 7, 12]. The operator Δ mediates the coupling to the electromagnetic field. In atomic units ($e = \hbar = m = 1, c = 137.036$) it follows:

$$\Delta = (1/2c) A_0 \cdot p. \tag{3}$$

A_0 denotes the spatially constant amplitude of the electromagnetic vector potential and p the momentum operator. In the case of photoemission ϵ_f is the single-particle

energy of the outgoing electron and $k_{\|}$ denotes its wavevector component parallel to the surface.

In general we have for the surface contribution of the current the formula

$$I^{\mathrm{surf}}(k_{\|}, \epsilon_{\mathrm{f}}) = -\frac{1}{\pi}\mathrm{Im}\int \langle k_{\|}, \epsilon_{\mathrm{f}}|G_2^{+}|r\rangle \Delta \langle r|G_1^{+}\Delta^{\dagger}G_2^{-}|\epsilon_{\mathrm{f}}, k_{\|}\rangle \,\mathrm{d}r \tag{4}$$

derived from equation (2).

In the region between the surface barrier and the first layer of the bulk crystal the wavefields for the initial and final states can be written in plane-wave representations, since it is assumed, that the potential is constant between the non-overlapping muffin-tin-spheres and the surface barrier potential $V_{\mathrm{B}}(z)$. The plane wave representation gives for the initial state

$$\langle r|G_1^{+}\Delta^{\dagger}G_2^{-}|\epsilon_{\mathrm{f}}, k_{\|}\rangle = \sum_{g}\left([a_{1g}^{+} + r_{1g}d_{1g}^{-}]\mathrm{e}^{\mathrm{i}k_{1g}^{+}(r-c_1)} + d_{1g}^{-}\mathrm{e}^{\mathrm{i}k_{1g}^{-}(r-c_1)}\right) \tag{5}$$

and for the final state

$$\langle k_{\|}, \epsilon_{\mathrm{f}}|G_2^{+}|r\rangle = \sum_{g}\left(u_{1g}^{+}\mathrm{e}^{\mathrm{i}k_{2g}^{+}(r-c_1)} + u_{1g}^{-}\mathrm{e}^{\mathrm{i}k_{2g}^{-}(r-c_1)}\right). \tag{6}$$

With the coefficient a_{1g}^{+}, which is emitted by the barrier, we take into account the reflection of the initial state wavefield by the surface potential. r_{1g} denotes the barrier-reflection coefficient for the hole-state.

According to the z-dependence of the barrier potential we have to calculate the initial and final state wavefield numerically in the surface region. It follows for the initial state

$$\langle r|G_1^{+}\Delta^{\dagger}G_2^{-}|\epsilon_{\mathrm{f}}, k_{\|}\rangle = \sum_{g}\phi_{1g}(z)\mathrm{e}^{\mathrm{i}k_{1g\|}(r-c_1)_{\|}} \tag{7}$$

with

$$\phi_{1g}(c_{1z}) = a_{1g}^{+} + r_{1g}d_{1g}^{-} + d_{1g}^{-} \tag{8}$$

and again for the final state

$$\langle k_{\|}, \epsilon_{\mathrm{f}}|G_2^{+}|r\rangle = \sum_{g}\psi_{2g}(z)\mathrm{e}^{\mathrm{i}k_{2g\|}(r-c_1)_{\|}} \tag{9}$$

with

$$\psi_{2g}(c_{1z}) = u_{1g}^{+} + u_{1g}^{-}. \tag{10}$$

Here ϕ_{1g} and ψ_{2g} denote the regular solutions of the Schrödinger equation for $V_{\mathrm{B}}(z)$ in the range $-\infty < z < c_{1z}$. The value c_{1z} defines the point, where the surface potential goes smoothly into the inner potential of the bulk crystal.

Inserting (7) and (9) into equation (4) and rewriting the surface contribution for the current, we arrive at the following expression:

$$I^{\mathrm{surf}}(k_{\|}, \epsilon_{\mathrm{f}}) = -\frac{1}{\pi}\frac{A_z}{2\omega c}\mathrm{Im}\left(\mathrm{e}^{\mathrm{i}q_{\|}\cdot c_{\|}}\sum_{g}\int_{-\infty}^{c_{1z}}\mathrm{d}z\,\psi_{2g}(z)\frac{\mathrm{d}V_{\mathrm{B}}}{\mathrm{d}z}\phi_{1g}(z)\mathrm{e}^{\mathrm{i}q_z z}\right) \tag{11}$$

where A_z is the z-component of the amplitude A_0 and q is the wavevector of the photon field.

The problem that remains, is the calculation of the coefficient a_{1g}^+, which belongs to the initial state wavefield emitted by the surface barrier. The initial state matrix element $\langle r|G_1^+\Delta^\dagger G_2^-|\epsilon_f, k_\parallel\rangle$ can be manipulated to a form more appropriate to a direct calculation:

$$\langle r|G_1^+\Delta^\dagger G_2^-|\epsilon_f, k_\parallel\rangle = \int \langle r|G_1^{+(0)} + G_1^{+(0)} r_1 G_1^{+(0)}|r'\rangle \Delta^\dagger \langle r'|G_2^-|\epsilon_f, k_\parallel\rangle \, \mathrm{d}r' \qquad (12)$$

where $G_1^{+(0)}$ is the free electron Green function for the initial state. After integrating over $\mathrm{d}r'_\parallel$ in equation (12), we can describe the matrix element by a plane wave expansion, which is valid in the region of our interest, namely between the surface barrier and the first bulk layer:

$$\langle r|G_1^+\Delta^\dagger G_2^-|\epsilon_f, k_\parallel\rangle = \sum_g a_{1g}^+ \mathrm{e}^{\mathrm{i}k_{1g}^+(r-c_1)} \qquad (13)$$

with

$$a_{1g}^+ = -\frac{\mathrm{i}A_z \mathrm{e}^{-\mathrm{i}q\cdot c_1}}{2\omega c k_{1gz}^+}(1 + r_{1g}) \int_{-\infty}^{c_{1z}} \mathrm{d}z \mathrm{e}^{-\mathrm{i}(q_z + k_{1gz}^+)(z-c_{1z})} \frac{\mathrm{d}V_B}{\mathrm{d}z} \psi_{2g}(z). \qquad (14)$$

For a step barrier $V_B(z) = V_{0r}\Theta(z - c_{1z})$, where Θ is the unit step function, we obtain Pendry's result [5]. V_{0r} denotes the constant inner potential of the bulk crystal.

In calculating the matrix element for the surface contribution by itself we follow Pendry's original ansatz. The main effect from a z-dependent surface barrier results in a strong variation of the barrier reflection coefficient r_{1g}. For that reason we use for the evaluation of this coefficient a potential model for $V_B(z)$, which has been introduced first by Rundgren and Malmström [13] in LEED calculations.

3. Results for Cu surfaces and discussion

The spectra of electronic surface states on Cu surfaces have been calculated with the theoretical model of section 2. For the bulk muffin-tin potential of Cu the potential due to Chodorow [14,15] was used. Damping processes within the one-step model are described by adding a constant imaginary part V_{0i} to the inner potential V_{0r}. For the high-lying electron states we took $V_{0i2} = -1$ eV, which is in accordance with LEED experience, for the low-lying states near E_F V_{0i1} was chosen as a small quantity $V_{0i1} = -0.02$ eV.

3.1. Cu(100)

In figure 1 we present the projected bulk bandstructure for Cu(100) together with all calculated and experimentally observed IPE data. The shape of the surface barrier [13]

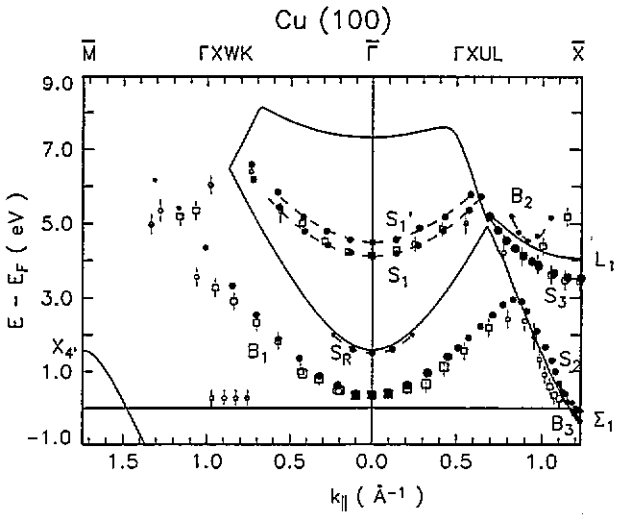

Figure 1. Bulk bandstructure of Cu, projected onto the $\bar{\Gamma}$–$\bar{X}$ and $\bar{\Gamma}$–$\bar{M}$ directions of the surface Brillouin zone. Solid circles (open squares with error bars) denote calculated (measured) band dispersions. The size of the symbol indicates the intensity of the transition. The band gaps of the projected bulk band structure are bounded by solid lines.

giving rise to the surface states S in figure 1 will be discussed below in a systematic comparison of all three low-index surfaces of Cu.

In addition to our former work on surface states at Cu(100) [8,16], which concentrated on the ΓXUL azimuth, here we give also the results for ΓXWK. Along ΓXUL so far four empty surface states SR, S_1, S_2, S_3 and two unoccupied bulk states B_1, B_2 have been detected in IPE experiments. SR denotes a crystal-induced surface resonance, S_1 the first image-potential state, both being associated with the $X_{4'}$–X_1 gap. S_2 and S_3 represent crystal-induced surface states derived from the $L_{2'}(\Sigma_1)$–L_1 gap. S_2 becomes an occupied surface state near $\bar{X}$ and has been detected there in high-resolution photoemission spectroscopy [17].

When compared to our former work [8, 16], an interesting new feature in figure 1 is the existence of an additional bulk state B_3 at −0.35 eV ($\bar{X}$) in the occupied regime near $\bar{X}$. This state lies at $\bar{X}$ 0.28 eV below S_2 and just at the Σ_1 bulk edge. In our former work [8,16] B_3 did not show up for two reasons. Those calculations had been restricted to the energy range above −0.1 eV, since no additional state had been expected. Moreover, those calculations concentrated on the z-component A_z of the photon field A_0. For B_3 it turns out, however, that the calculated orientation of the electric dipole axis in the ΓXUL azimuth is rotated $\sim 45°$ away from the surface normal. In a pure z-polarized spectrum B_3 therefore becomes suppressed.

The question, whether B_3 has been observed in corresponding high resolution photoemission experiments [17] in addition to S_2, is not clear. In these experiments a doublet of surface states S′,S is seen both for excitation energy $\hbar\omega = 16.85$ eV (NeI) and $\hbar\omega = 11.85$ eV (ArI), but the presence of the second component S′ was attributed to the NeI ($\Delta = 0.177$ eV) and ArI ($\Delta = 0.210$ eV) satellite line in the exciting photon field. This satellite splitting, however, is comparable to the calculated B_3–S_2 splitting in the occupied regime which is of the order of 0.15–0.28 eV. Moreover, the fact that both energetic separation and relative intensity in the S′,S doublet vary slightly in the experiment as a function of Θ (cf figure 2 in [17]) suggests that the existence of an additional state near $\bar{X}$ might be a real effect.

Typical calculated IPE-spectra and corresponding experimental data ($\hbar\omega = 9.7$ eV) for different angles Θ of electron incidence and photons emitted within the azimuth

in different directions α with respect to the surface normal z are shown in figure 2 for ΓXUL and in figure 3 for ΓXWK, respectively. The spectra are raw spectra, convoluted with a Gaussian of 0.275 eV full width at half-maximum, to take the experimental resolution into account. Apart from the fact that the experimental spectra show a large fraction of secondary emitted photons, which are not taken into account in the calculations, the agreement between theory and experiment is generally very good. In particular the polarization dependence of the intensity of the various peaks is well reproduced in the theory

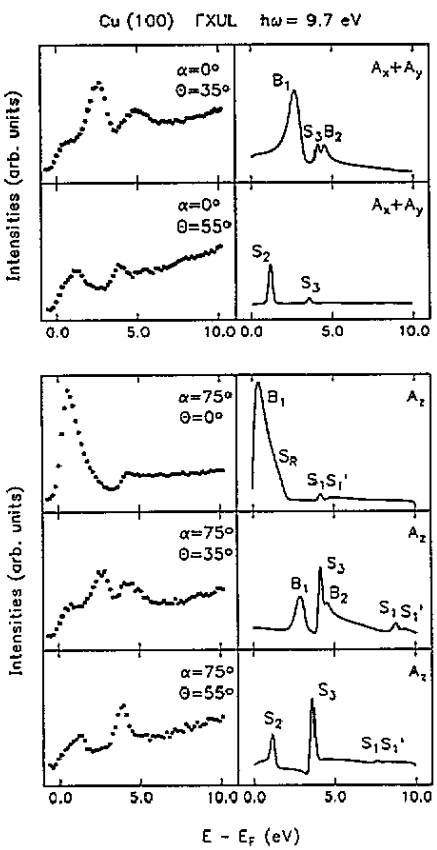

Figure 2. Experimental (left) and theoretical (right) inverse photoemission spectra ($\hbar\omega$ = 9.7 eV) for Cu(100) along the ΓXUL bulk mirror plane. Θ denotes the angle of electron incidence and α the photon detection angle.

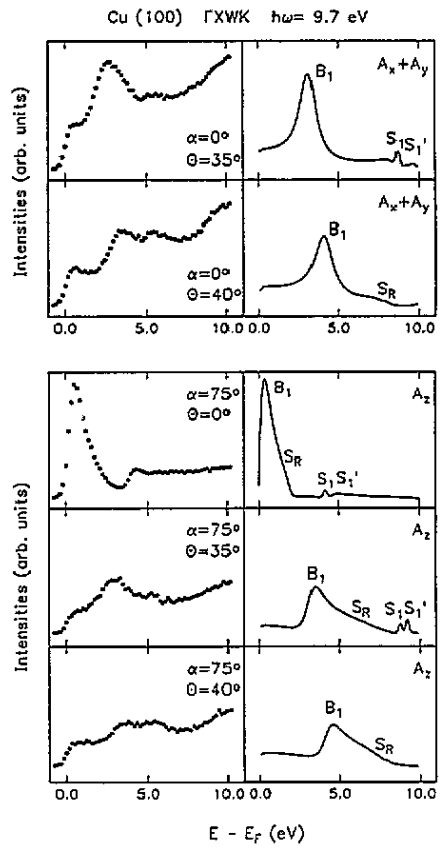

Figure 3. Experimental (left) and theoretical (right) inverse photoemission spectra ($\hbar\omega$ = 9.7 eV) for Cu(100) along the ΓXWK bulk mirror plane. Θ denotes the angle of electron incidence and α the photon detection angle.

A systematic comparison of all calculated surface states at the zone centre $\bar{\Gamma}$ and boundary $\bar{X}$ with experimental data for Cu(100) is included in table 1. The agreement between theory and experiment for the energetic positions and effective masses is within the error bars of the experiment. A recent inverse photoemission study of Cu(100) at variable photon energy reported a surface state at the zone boundary $\bar{X}$ with energy $\simeq 0.5$ eV [18] (not included in table 1). We have calculated the corresponding IPE spectrum ($\hbar\omega$ = 22.7 eV), but have been unable to find a

surface state at $\bar{X}$ in this energy range. At present the origin of this discrepancy is not clear.

Table 1. Comparison of experimental and calculated binding energies and effective masses of surface states on Cu(100), Cu(110) and Cu(111).

Surface normal	Symmetry point	Type	$E - E_F$ (eV) (theory)	m^*/m_e (theory)	$E - E_F$ (eV) (experiment)	m^*/m_e (experiment)	Reference
					4.13 ± 0.20		[41]
(100)	$\bar{\Gamma}$	S_1	4.10	0.990	4.00 ± 0.20	1.2 ± 0.20	[37]
					4.06 ± 0.02	0.90 ± 0.10	[42]
(100)	$\bar{\Gamma}$	S_1'	4.48	1.010	4.45 ± 0.02		[42]
					1.15		[45]
(100)	$\bar{\Gamma}$	S_R	1.50	0.427	1.20 ± 0.30		[41]
					1.48 ± 0.06		[44]
(100)	$\bar{X}$	S_2	−0.065	0.076	-0.058 ± 0.025	0.067 ± 0.01	[17]
(100)	$\bar{X}$	S_3	3.52	0.630	3.60 ± 0.20	0.70 ± 0.20	[36]
					3.45 ± 0.20		[41]
(110)	$\bar{\Gamma}$	S_1	4.54	0.98	4.28 ± 0.35		[40]
					4.39 ± 0.15		[43]
(110)	$\bar{\Gamma}$	S_1'	4.74	0.99			
(110)	$\bar{Y}$	S_2	−0.42	0.21	-0.393 ± 0.025	0.268 ± 0.01	[19]
					2.50 ± 0.20	1.10	[35]
(110)	$\bar{Y}$	S_3	2.38	0.94	1.91 ± 0.25		[41]
					1.80 ± 0.20	0.80 ± 0.20	[39]
(110)	$\bar{X}$	S_4	1.96	0.248	2.09 ± 0.20		[41]
					2.00 ± 0.40		[40]
(110)	$\bar{X}$	S_5	5.36	1.49	5.63 ± 0.20		[41]
					5.40 ± 0.40		[39]
					4.11 ± 0.03		[21]
(111)	$\bar{\Gamma}$	S_1	4.06	0.89	4.05 ± 0.05	1.00 ± 0.10	[22]
					4.39 ± 0.20		[41]
(111)	$\bar{\Gamma}$	S_1'	4.68	0.98	4.63 ± 0.05	0.90 ± 0.15	[22]
(111)	$\bar{\Gamma}$	S_2	−0.40	0.369	-0.389 ± 0.025	0.462 ± 0.01	[20]
					-0.39 ± 0.02	0.46	[21]
(111)	$\bar{M}, \bar{M}'$	S_3	0.98	0.031			

By definition a surface state must contribute to the surface current I^{surf} in equation (11), i.e. its intensity for z-polarized light should be non-zero. Mirror symmetry of the three low-index surfaces in FCC crystals then induces that for a surface state at $\bar{\Gamma}$ the intensity for x- or y-polarized light must vanish as long as spin–orbit interaction is disregarded. In such a case the dipole orientation Θ_z of the surface state thus will be exactly parallel to z, i.e. $\Theta_z = 0°$. Here Θ_z denotes the angle between the vector formed from $I(A_x)$, $I(A_y)$, $I(A_z)$ and the surface normal. Similiarly for a surface state in an azimuth, which represents a mirror plane of the crystal, the intensity for y-polarized light perpendicular to the azimuth must vanish. The vector formed from $I(A_x)$, $I(A_y)$, $I(A_z)$ thus will lie within the mirror plane, but its orientation Θ_z for a surface state away from $\bar{\Gamma}$ can in principle now span the range $0° \leqslant \Theta_z < 90°$. Increasing values of Θ_z then indicate an increasing bulk

contribution to the surface state. In our calculation for Cu(100) we found significant non-zero values of Θ_z only for the surface state S_2 at $\bar{X}$. This result shows that this state could be sensitive to corrugation in the effective barrier potential $V_B(\mathbf{r})$ of equation (1), an effect which is not taken into account here.

In addition to the transitions discussed so far, the experimental IPE-spectra contain dispersionsless features in the range 0–1.5 eV above the Fermi level. These features, which show up at all three low-index surfaces of Cu, must be attributed to transitions into weak maxima of the three-dimensional density-of-states (DOS) in this energy range.

3.2. Cu(110)

The projected bulk bandstructure for Cu(110) together with all calculated and experimentally observed IPE data is shown in figure 4. In addition to the first and second image-potential states S_1 and S_1' near $\bar{\Gamma}$, two crystal-induced surface states S_2, S_3 (ΓKLU) and S_4, S_5 (ΓKWX) are clearly identified in the $L_{2'}$–L_1 and $X_{4'}$–X_1 derived band gaps. Furthermore three unoccupied bulk states B_1, B_2, B_3 have been detected in IPE experiments. In analogy to the (100) surface, S_2 becomes an occupied surface state near $\bar{Y}$ and has been detected there in high-resolution photoemission spectroscopy [19].

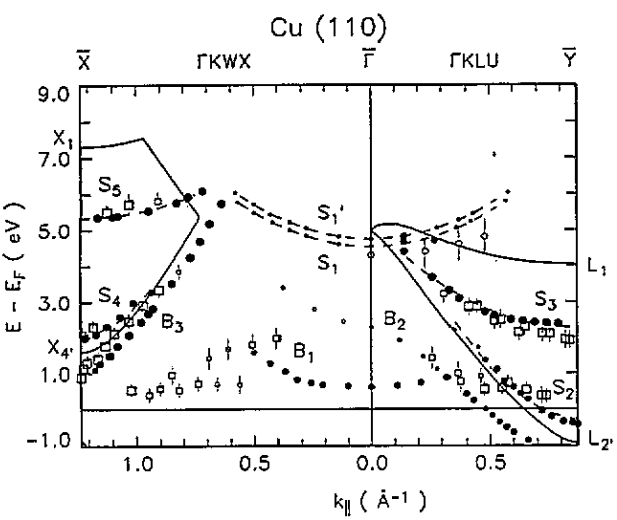

Figure 4. Bulk bandstructure of Cu, projected onto the $\bar{\Gamma}$–$\bar{X}$ and $\bar{\Gamma}$–$\bar{Y}$ directions of the surface Brillouin zone. Solid circles (open squares with error bars) denote calculated (measured) band dispersions. The size of the symbol indicates the intensity of the transition. The band gaps of the projected bulk band structure are bounded by solid lines.

Calculated IPE-spectra and measured data ($\hbar\omega = 9.7$ eV) are shown in figure 5 for the ΓKLU azimuth and in figure 6 for ΓKWX. Theory and experiment agree very well. As in the case of Cu(100) the peaks in the experimental spectra are often obscured by a large fraction of secondary emitted photons. Energy and effective mass of all surface states at Cu(110) are included in table 1. With the exception of the second image-potential state S_1' at $\bar{\Gamma}$, which so far has not been observed experimentally, we find essentially agreement between theory and experiment within the experimental error bars. Significant non-zero values for the electric dipole orientation Θ_z of surface states at Cu(110) were found for $S_2(\bar{Y})$ and $S_4(\bar{X})$, i.e. these states could also be sensitive to corrugation effects in the effective barrier potential.

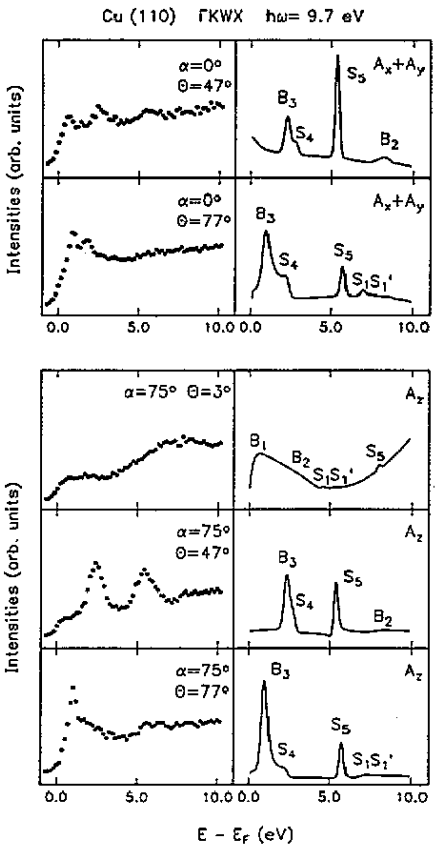

Figure 5. Experimental (left) and theoretical (right) inverse photoemission spectra ($\hbar\omega$ = 9.7 eV) for Cu(110) along the ΓKWX bulk mirror plane. Θ denotes the angle of electron incidence and α the photon detection angle.

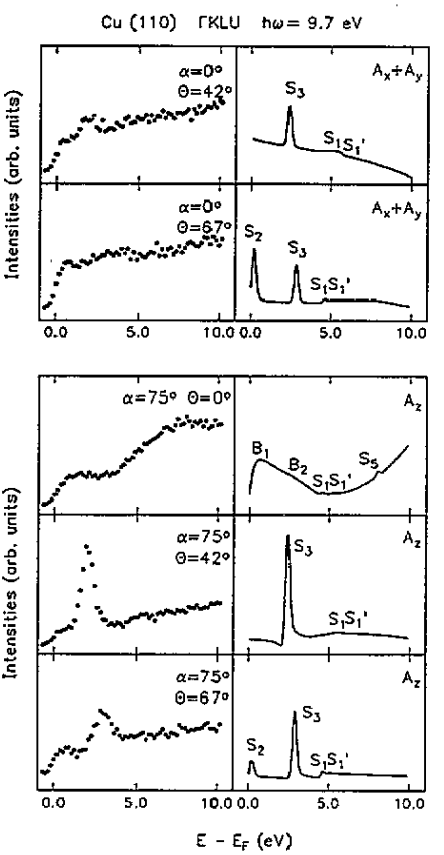

Figure 6. Experimental (left) and theoretical (right) inverse photoemission spectra ($\hbar\omega$ = 9.7 eV) for Cu(110) along the ΓKLU bulk mirror plane. Θ denotes the angle of electron incidence and α the photon detection angle.

3.3. Cu(111)

Figure 7 shows the projected bulk bandstructure for Cu(111) together with all calculated and experimentally observed IPE data. Three bulk states B_1, B_2, B_3, two image-potential surface states S_1, S_1' above the $L_{2'}$–L_1 derived gap and two crystal-induced surface states S_2, S_3 in the $L_{2'}$–L_1 and $X_{4'}$–L_1 derived gap are identified. Again S_2 becomes an occupied surface state near $\bar{\Gamma}$ and is observable in high-resolution photoemission spectroscopy [20,21].

The ΓXUL and ΓLKL azimuths shown in figure 7 are equivalent, if only the surface layer is taken into account, but become non-equivalent for the bulk crystal. Pure surface states thus should behave symmetrically in both azimuths, whereas bulk states can exhibit an asymmetry. This is indeed the case in figure 7. For the surface states this means that the dipole orientation Θ_z is nearly zero up to the zone boundary. For the Cu(111) surface there is thus no indication for corrugation effects in the effective barrier potential, a result which is compatible with the densely packed structure of this surface.

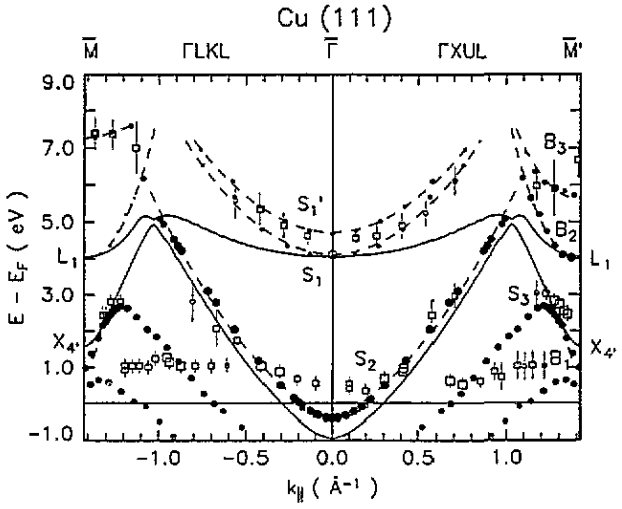

Figure 7. Bulk bandstructure of Cu, projected onto the $\bar{\Gamma}$–$\bar{M}$ and $\bar{\Gamma}$–$\bar{M}'$ directions of the surface Brillouin zone. Solid circles (open squares with error bars) denote calculated (measured) band dispersions. The size of the symbol indicates the intensity of the transition. The band gaps of the projected bulk band structure are bounded by solid lines.

Calculated IPE-spectra and measured data ($\hbar\omega = 9.7$ eV) for Cu(111) are shown in figures 8 and 9 for the azimuths ΓXUL and ΓLKL, respectively. Again theory and experiment agree very well. The non-equivalence of both azimuths for bulk states is clearly seen. In addition this non-equivalence also exists for larger values of Θ, i.e. near the zone boundary, in the intensity of the surface state S_3. In fact $S_3(\bar{M}, \bar{M}')$ exhibits the largest non-zero value for the dipole orientation ($\Theta_z = 3.9°$) among the surface states at Cu(111). Energy and effective mass of surface states at Cu(111) are included in table 1 and again show an agreement with the experiment essentially within experimental error bars. Note that the energetic position of S_3 at the zone boundary is not known exactly. Like in the case of Cu(100) and Cu(110) the experimental IPE data show weak dispersionsless features in the energy range 0.5–1.5 eV above the Fermi level which correspond to DOS transitions.

3.4. Corrugation effects

In the present paper corrugation is defined as the lateral variation of the barrier potential $V_B(r)$ in equation (1) with $r_{\|}$. This effect is neglected in our calculations. Note, however, that the total bulk crystal potential will exhibit a trivial lateral variation and that this effect is of course taken into account by our formalism.

The relative importance of corrugation in the barrier potential can be judged by inspection of the angles Θ_z of the dipole orientation of the various surface states. The maximum Θ_z values at the various surfaces are: $\Theta_z = 10.3°$ for $S_4(\bar{X})$ at Cu(110), $\Theta_z = 9.5°$ for $S_2(\bar{X})$ at Cu(100) and $\Theta_z = 3.9°$ for $S_3(\bar{M}, \bar{M}')$ at Cu(111). The relative importance of corrugation thus decreases with increasing density of atoms in the surface unit cell. This was to be expected.

To judge the absolute importance of corrugation effects in the barrier, it is necessary to resort to the occupied surface state S_2 at the various surfaces, since this state has been measured with the highest resolution. A comparison of theory and experiment for S_2 is shown in figure 10. The calculated energetic position of S_2 at the various symmetry points is always within the error bars of the experiment. Only the calculated effective mass of S_2 at Cu(110) and Cu(111) lies slightly outside the

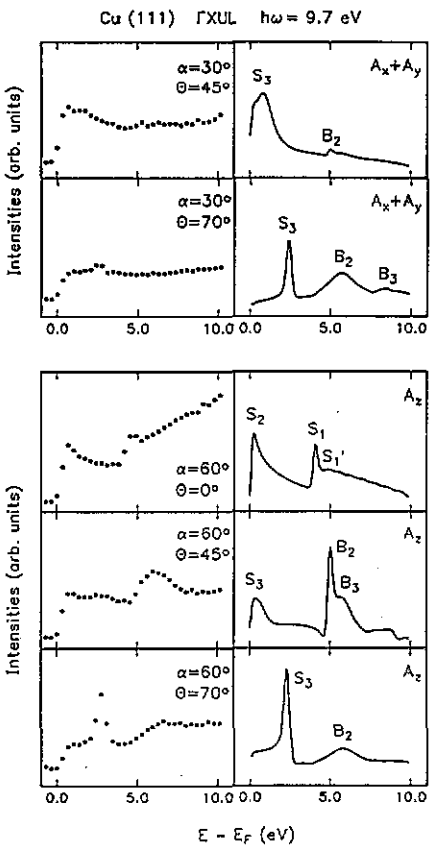

Figure 8. Experimental (left) and theoretical (right) inverse photoemission spectra ($\hbar\omega = 9.7$ eV) for Cu(111) along the ΓXUL bulk mirror plane. Θ denotes the angle of electron incidence and α the photon detection angle.

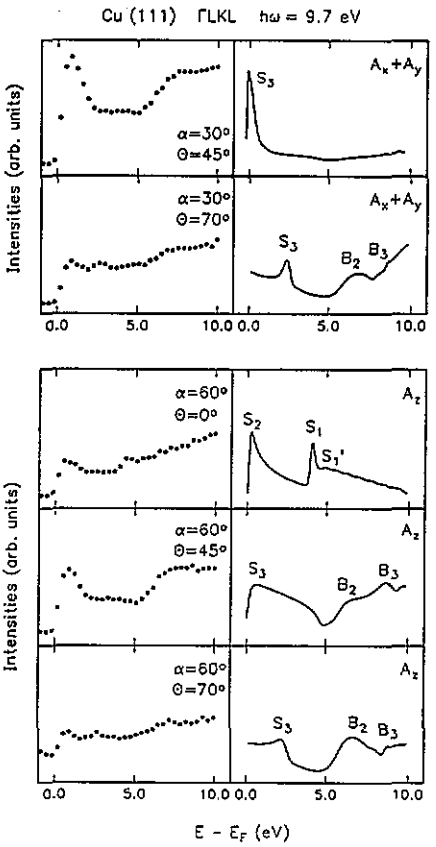

Figure 9. Experimental (left) and theoretical (right) inverse photoemission spectra ($\hbar\omega = 9.7$ eV) for Cu(111) along the ΓLKL bulk mirror plane. Θ denotes the angle of electron incidence and α the photon detection angle.

error bars, but we hesitate to interpret this as a clear-cut indication for the importance of surface corrugation.

Another group of surface states, which is known with high precision, are certain image-potential states, which are accessible to two-photon photoemission. In the case of Cu this is the case for S_1 and S_1' at the (100) and the (111) surface [21, 22, 42]. From the agreement between theory and experiment in table 1 for these states we conclude, that an influence of surface corrugations is not detectable in these cases. This conjecture is in agreement with a recent theoretical study of this problem [11].

3.5. Effective surface barrier

The effective z-dependent surface barriers $V_B(z)$ for the various Cu surfaces are shown in figure 11. They are plotted with respect to the vacuum level E_{vac} utilizing the values of the work function Φ as given in table 2. The zero of the z scale lies in the uppermost layer of atoms. As mentioned above, $V_B(z)$ is of the Rundgren–Malmström (RM) type [13]. For its real part we have:

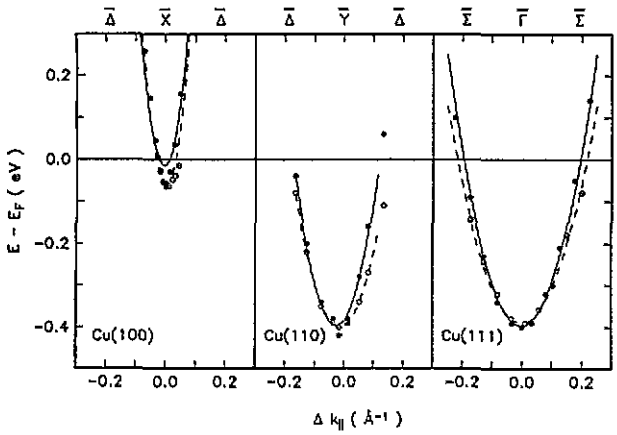

Figure 10. Bulk bandstructure of Cu, projected onto the $\bar{\Gamma}$–$\bar{X}$, $\bar{\Gamma}$–$\bar{Y}$ directions of the surface Brillouin zone near $\bar{X}$, $\bar{Y}$ and near $\bar{\Gamma}$ in the $\bar{\Gamma}$ – $\bar{M}(\bar{M}')$ direction. Solid (open) circles denote calculated (measured) band dispersions.

$$V_B(z) = \begin{cases} \frac{1}{4}(z - z_{im})^{-1} & z < z_A < z_{im} \\ s_0 + s_1(z - z_A) + s_2(z - z_A)^2 + s_3(z - z_A)^3 & z_A < z < z_E \\ V_{or} & z > z_E \end{cases} . \quad (15)$$

Here z_{im} denotes the position of the classical image plane. The asymptotic regime $z < z_A$ is connected to the bulk muffin-tin zero V_{or} by a third-order polynomial in z, spanning the range $z_A < z < z_E$. The polynomial coefficients s_0, s_1, s_2, s_3 are fixed through the requirement of continuity of $V_B(z)$ and its derivative. The parameters z_{im}, z_A, z_E, the polynomial range $\Delta z = |z_A - z_E|$, the size A_E of the surface unit cell and one-half of the interlayer distance $d_{1/2}$ are listed in table 2 for the various surfaces.

Table 2. Potential parameters for the barrier potentials of Cu(111), Cu(100) and Cu(110).

	Cu (111)	Cu (100)	Cu (110)
Workfunction: Φ (eV)	4.88	4.63	4.87
Reference	[43]	[38]	[43]
Surface barrier potential: V_{or} eV	−12.43	−12.18	−12.42
Beginning of the polynomial region: z_A a.u.	−3.611	−3.974	−4.066
End of the polynomial region: z_E a.u.	−0.522	−0.008	0.577
Length of the polynomial region: $\Delta z = \|z_A - z_E\|$ a.u.	3.089	3.966	4.643
Size of the surface unit cell: A_E 10^{-2} a.u.^{2}	0.722	0.833	1.179
One-half of interlayer distance: $d_{1/2}$ a.u.	−1.972	−1.708	−1.206
Position of the image plane: z_{im} a.u.	−2.047	−1.932	−1.762

The shape of the surface barrier depends on the parameters z_{im}, z_A, z_E that were determined in the following manner. To receive an approximate value for the

position of the image plane z_{im}, we started the variational procedure with one-half of the interlayer distance $d_{1/2}$ and fixed the value for z_{im} roughly by comparison of the experimental and theoretical peak positions for normal emission ($k_{||} = 0$). In determining the beginning z_A and the end of the polynomial region z_E, these parameters were varied from +1.0 to −5.0 a.u. In this way, as well as for the exact fixing of z_{im}, the peak positions and effective masses of all surface states in the whole projected bulk bandstructure were taken into account, to receive the best fit for the surface potential. The quality of the surface potential depends on the accuracy of the experimental measurements. To reproduce the measured data within the experimental resolution, especially the results from the high resolution photoemission experiments [17,19,20] and two-photon photoemission experiments [21,22,42,44], it was necessary to vary the most sensitive parameter z_{im} up to the third digit.

It should be noted that no relaxation of the outermost atomic surface layer has been taken into account in the present calculation. This neglection of relaxation effects seems to be justified on the basis of various thin film calculations for Cu surfaces and LEED fine structure analysis cited below.

From the data in table 2 it is seen, that z_{im} moves toward the first layer of atoms and the polynomial range Δz becomes larger, if A_E increases. This means, that the most open surface, Cu(110), exhibits the strongest saturation of the image potential with an image plane lying nearest to the topmost layer. As a further consequence the image force for a given value of z outside the crystal is strongest for Cu(111) and weakest for Cu(110).

This behaviour is in agreement with calculated surface barrier parameters for the semi-infinite jellium model for varying density of the conduction electrons [23–25]. Moreover it agrees with the results of density functional calculations for thin films of Cu(100) and Cu(110) [26,27]. However, the absolute value of z_{im} for Cu surfaces in these calculations was significantly larger than in the present study. For Cu(100) the results are $z_{im} = -2.40$ a.u. [26], −2.33 a.u. [27] compared to −1.93 a.u. in table 2, for Cu(110) $z_{im} = -2.17$ a.u. [26], −2.28 a.u. [27] compared to our result −1.76 a.u.

It has been argued [26] that this systematic deviation is due to different choices of the barrier model. In fact in the calculations of [26,27] the self-consistent static effective potential of LDA–DFT in the surface region was planar-averaged and then fitted to an expression (JJJ) [28]

$$V_B(z) = \begin{cases} \dfrac{1}{4(z - z_{im})}\{1 - \exp[\lambda(z - z_{im})]\} & z < z_{im} \\ -V_{or}/\{A \exp[-B(z - z_{im})] + 1\} & z > z_o. \end{cases} \tag{16}$$

Here A and B are constants determined by matching $V_B(z)$ and its derivative at the image plane $z = z_{im}$.

We have also used the JJJ barrier in our calculations for Cu(100). With parameters $V_{or} = -0.896$ Ry, $z_{im} = -1.93$ a.u., $\lambda = 1.34$ one obtains a description of all surface states at Cu(100), which is of similiar accuracy as that discussed in subsection 3.3 on the basis of the RM barrier. The conjecture, that the JJJ and RM barriers result in similiar values for z_{im}, when fitted to the same data base, is furthermore corroborated by recent work of Smith *et al* [27]. These authors fitted the JJJ barrier for the various Cu surfaces to corresponding surface state energies, making use of a simple phase-accumulation model. The simplicity of this model does not allow for the derivation of a definite set of barrier parameters, which works for all observed surface states

at a given surface. What can be obtained, however, are parameters averaged over the surface states included in the fitting procedure. In this way the authors derived $\langle z_{im} \rangle = -2.27$ a.u. for Cu(111), $\langle z_{im} \rangle = -2.18$ a.u. for Cu(100) and $\langle z_{im} \rangle = -1.70$ a.u. for Cu(110). One notices that these JJJ fits to the experiment still yield values for z_{im} smaller than the corresponding JJJ fits to the theoretical potentials in [26,27]. Moreover, these averaged parameters are in very nice agreement with our RM fits to a data base of similiar quality. The fact, that the face dependence in these $\langle z_{im} \rangle$ values is more pronounced than in our z_{im} parameters, is understandable, since the two procedures work at quite different levels of theoretical refinement.

The differences in z_{im} between fits to calculated first-principles LDA–DFT potentials and fits to experimental surface state data are therefore likely to have a different origin. In the introduction we have already mentioned that the effective potential felt by an electron in the surface region is in principle energy-dependent. The height $|V_{or}|$ of the surface barrier decreases with increasing electron energy. The effective potential thus become less attractive and the effective image plane position z_{im} shifts toward the crystal, if the electron moves [29].

Such dynamical effects could in principle explain the above mentioned differences in z_{im}. There is, however, a caveat: a recent very careful analysis of LEED fine structure data of Cu(001), using the JJJ barrier with V_{or} as a parameter, resulted in $z_{im} = -2.5 \pm 0.1$ a.u. [30]. An earlier LEED fit to the JJJ barrier of Cu(001) had given -2.35 a.u. [31]. From a comparison of these experimental fits with the fits to the theoretical potentials in [26,27] an inward shift of z_{im} as a consequence of dynamical effects cannot be deduced. Since the electron energies in such LEED fine structure experiments are usually larger than those of electrons occupying bound surface states above the Fermi level, the same would then be true for the interpretation of the corresponding IPE data. The conjecture, that dynamical effects in the effective potential should become non-neglectible only for energies significantly above the vacuum level, is supported by our analysis of high lying unoccupied bulk states ($E - E_F \simeq 10$–15 eV) in the following paragraph.

We believe that the above mentioned discrepancies in z_{im} between theory and experiment have their origin mainly in the way in which the presence of an image tail is enforced in the theoretical analysis. Fitting an *ab-initio* LDA–DFT barrier with incorrect asymptotic behaviour to a model barrier with correct behaviour [26,27] is a problematic task. A strategy to determine z_{im} from an *ab-initio* DFT barrier with correct asymptotics is clearly preferable, but so far such calculations seem to exist only for the semi-infinite jellium model [32,33] and not for real metal surfaces.

3.6. High-lying unoccupied bulk states

In figure 12 we show calculated IPE spectra and corresponding experimental data ($\hbar\omega = 9.7$ eV) for unoccupied bulk states of various Cu surfaces in the energy range 10–15 eV above the Fermi level. In these calculations we used $V_{0i1} = -0.1$ eV, $V_{0i2} = -2.0$ eV to account for the higher energy range. A comparison between theory and experiment shows good agreement with respect to the shape of the various spectra. The energetic positions are, however, systematically shifted by 0.5–2.5 eV in the sense, that the experimental peaks lie at higher energies above the Fermi level. We interpret this systematic effect as a consequence of dynamical effects in the effective one-electron potential felt by an electron in such an unoccupied bulk orbital. This explanation is supported by similiar work of Speier *et al* [34]. These authors compared measured IPE peaks in an energy range 5–50 eV above the Fermi level

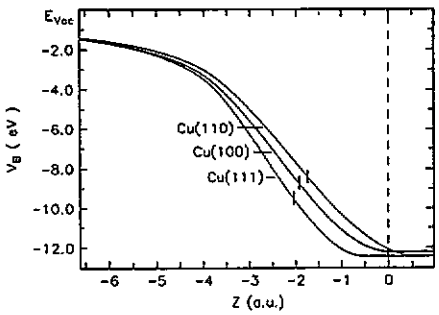

Figure 11. Barrier potentials for Cu(111), Cu(100) and Cu(110) from analysis of inverse photoemission, photoemission and two photon photoemission data. The origin $z = 0$, marked by the dotted line, represents the centre of the first row of atoms. The different image planes are marked by solid short lines.

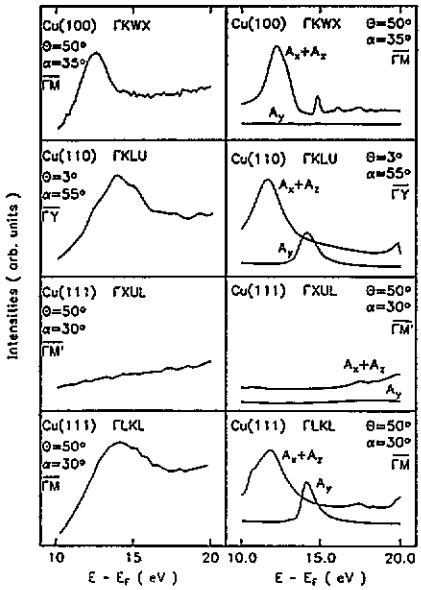

Figure 12. Experimental (left) and theoretical (right) inverse photoemission spectra for high-lying unoccupied bulk states ($\hbar\omega = 9.7$ eV) for Cu(100), Cu(110) and Cu(111) along the ΓKWX, ΓYLU, ΓXUL and ΓLKL directions. Θ denotes the angle of electron incidence and α the photon detection angle.

with calculated peaks in the density of states for various transition and noble metals, including Cu. Their conclusion was, that for Cu dynamical effects in the effective potential are negligible up to 6 eV above the Fermi level, but become of the order of 1 eV for states in the range 10–20 eV. Our result is in good agreement with their finding, though in our case the systematic shift is more pronounced. This may also be due to the different calculated muffin-tin potential entering the analysis.

4. Conclusions

The surface potential barrier shape of the low-index faces of copper can be determined by an analysis of inverse photoemission and two-photon photoemission measurements making use of the one-step model of photoemission. The barrier potentials derived here allow for a consistent description of the energetic positions and effective masses of all known surface states for the various faces. In agreement with previous theoretical predictions the most open surface, Cu(110), exhibits the strongest saturation of the image potential with an image plane lying nearest to the topmost layer. Theoretical *ab-initio* type slab calculations show the same trend, but in these calculations the position of the image plane is found significantly further outside the crystal. Corrugation and dynamical effects in the effective potential seem to be negligible for electronic states up to 6 eV above E_F.

Acknowledgment

Financial support of the Deutsche Forschungsgemeinschaft is gratefully acknowledged.

References

[1] Echenique P M and Pendry J B 1990 *Prog. Surf. Sci.* **32** 111
[2] Fetter A L and Walecka J D 1971 *Quantum-theory of many particle systems* (New York: McGraw-Hill)
[3] Lundqvist S and March N H 1983 *Theory of the inhomogeneous electron gas* (New York: Plenum)
[4] Jennings P J and Jones R O 1988 *Adv. Phys.* **37** 341
[5] Pendry J B 1976 *Surf. Sci.* **57** 679
[6] Pendry J B 1981 *J. Phys. C: Solid State Phys.* **14** 1381
[7] Hopkinson J F L, Pendry J B and Titterington D J 1980 *Comput. Phys. Commun.* **19** 69
[8] Borstel G and Thörner G 1988 *Surf. Sci. Rep.* **8** 1
[9] Inglesfield J E 1982 *Rep. Prog. Phys.* **45** 223
[10] Baribeau J M, Carette J D, Jennings P J and Jones R O 1985 *Phys. Rev.* B **32** 6131
[11] Van Siclen C DeW 1990 *Phys. Rev.* B **41** 8175
[12] Pendry J B 1974 *Low energy electron diffraction* (London: Academic)
[13] Malmström G and Rundgren J 1980 *Comput. Phys. Commun.* **19** 263
[14] Chodorow M I 1939 *Phys. Rev.* **55** 675
[15] Burdick G A 1963 *Phys. Rev.* **129** 138
[16] Thörner G and Borstel G 1986 *Appl. Phys.* A **41** 99
[17] Kevan S D 1983 *Phys. Rev.* B **28** 2268
[18] Lange C, Mandel T, Laubschat C and Kaindl G 1990 *J. Electron Spectrosc. Relat. Phenom.* **52** 49
[19] Kevan S D 1983 *Phys. Rev.* B **28** 4822
[20] Kevan S D 1983 *Phys. Rev. Lett.* **50** 526
[21] Fischer N, Schuppler S, Fischer R, Fauster Th and Steinmann W 1991 *Phys. Rev.* B **43** 14722
[22] Kubiak G D 1988 *Surf. Sci.* **201** L475
[23] Lang N D and Kohn W 1970 *Phys. Rev.* B **1** 4555
[24] Lang N D and Kohn W 1971 *Phys. Rev.* B **3** 1215
[25] Lang N D and Kohn W 1973 *Phys. Rev.* B **7** 3541
[26] Jennings P J, Jones R O and Weinert M 1988 *Phys. Rev.* B **37** 6113
[27] Smith N V, Chen C T and Weinert M 1989 *Phys. Rev.* B **40** 7565
[28] Jones R O, Jennings P J and Jepsen O 1984 *Phys. Rev.* B **29** 6474
[29] Weinert M, Hulbert S L and Johnson P D 1985 *Phys. Rev. Lett.* **55** 2055
[30] Hitchen G J, Thurgate S M and Jennings P J 1991 *Phys. Rev.* B **44** 3939
[31] Read M N 1985 *Appl. Surf. Sci.* **22/23** 48
[32] Ossicini S, Bertoni C M, and Gies P 1986 *Europhys. Lett.* **1** 661
[33] Eguiluz A G, Heinrichsmeier M, Fleszar A and Hanke W 1992 *Phys. Rev. Lett.* **68** 1359
[34] Speier W, Zeller R and Fuggle J C 1985 *Phys. Rev.* B **32** 3597
[35] Bartynski R A, Gustafson T and Soven P 1985 *Phys. Rev.* B **31** 4745
[36] Donath M, Glöbl M, Senftinger B and Dose V 1986 *Solid State Commun.* **60** 237
[37] Dose V, Altmann W, Goldmann A, Kolac U and Rogozik J, *Phys. Rev. Lett.* **52** 1919
[38] Giesen K, Hage F, Himpsel F J, Riess H J and Steinmann W 1987 *Phys. Rev.* B **35** 971
[39] Jacob W, Dose V, Kolac U, Fauster Th and Goldmann A 1986 *Z. Phys.* B **63** 459
[40] Reihl B and Frank K H 1985 *Phys. Rev.* B **31** 8282
[41] Schneider R, Dürr H, Fauster Th and Dose V 1990 *Phys. Rev.* B **42** 1638
[42] Steinmann W 1989 *Appl. Phys.* A **49** 365
[43] Straub D and Himpsel F J 1986 *Phys. Rev.* B **33** 2256
[44] Wegehaupt T, Rieger D and Steinmann W 1988 *Phys. Rev.* B **37** 10086
[45] Woodruff D P, Hulbert S L, Johnson P D and Smith N V 1985 *Phys. Rev.* B **31** 4046